Reference Plane based Fisheye Stereo Epipolar Rectification

Nobuyuki Kita and Yasuyo Kita
Intelligent Systems Research Institute, National Institute of Advanced Industrial Science and Technology (AIST),
Tsukuba Central 1, Tsukuba 305-8560, Japan
{n.kita, y.kita}@aist.go.jp

Keywords: Fisheye Stereo, Epipolar Rectification, Stereo Measurement, Humanoid Robot, Multi Contact, Near Support Plane.

Abstract: When a humanoid robot walks through or performs a task in a very narrow space, it sometimes touches the environment with its hand or arm to retain its balance. To do this the robot must identify a flat surface of appropriate size with which it can make sufficient contact; the surface must also be within reach of robot's upper body. Using fisheye stereo vision, it is possible to obtain image information for a field of view wider than that of a hemisphere whose central axis is the optical axes; thus, three dimensional distances to the possible contact spaces can be evaluated at a glance. To realize it, stereo correspondence is crucial. However, the short distance between the stereo cameras and the target space causes differences in the apparent shapes of the targets in the left and right images, which can make stereo correspondence difficult. Therefore, we propose a novel method which rectifies stereo images so that the targets have the same apparent shapes in the left and right images when the targets are close to a reference plane. Actual fisheye stereo image pairs were rectified, and three dimensional measurements were performed. Better results were obtained using the proposed rectification method than using other rectification methods.

1 INTRODUCTION

Humanoid robots are expected to substitute or support the work of humans in many places such as at disaster sites, airplane assembly plants, and building sites. As such, humanoid robots must be able to traverse narrow spaces and conduct tasks that require their upper body parts, e.g., hands, elbows, and shoulders, in addition to the soles of their feet to maintain their balance (Sentis, 2010), (Escande, 2013), (Henze, 2016). To realize such stabilization motions in unknown environments, a planar area which has proper sizes and poses have to be identified in the vicinity of the humanoid robot's upper body (Brossette, 2013), (Khatib, 2014). The measurements that are necessary to adequately evaluate the environment are as follows.

1. Dense three dimensional (3D) distance measurements.
2. 3D distance measurements in reach of the robot.
3. 3D distance measurements of the immediate vicinity of the humanoid robot's upper body.
4. Fast 3D distance measurements.
5. 3D distance measurements of poorly textured surfaces.

Various types of equipment have been developed for 3D distance measurements. The most popular is the RGB-D sensor (where the D represents the "depth" channel); this sensor can perform measurements 1, 4, and 5. Measurement 3 can be achieved by controlling the pose of a sensor. However, there are no off-the-shelf RGB-D sensors that can perform measurement 2. Most teams that signed-up for the DRC (Defense Advanced Research Projects Agency Robotics Challenge) in 2015 used a spinning LIDAR sensor, which is high-speed rotational 1D scanning type LRF (Laser rangefinder). This type of sensor can conduct measurements 1, 3, 4, and 5. However, the closest distance at which LRFs work is 0.5 m, which is too far to enable measurement 2 to be conducted. For a long time now, stereo vision that uses multiple cameras has been used for 3D distance measurements. There are numerous studies on stereo measurements and many available products. However, the width of the space these products can measure is limited because they usually use cameras with normal fields of view; thus, additional pose control equipment is necessary to carry out measurement 3.

Kita N. and Kita Y.
Reference Plane based Fisheye Stereo Epipolar Rectification.
DOI: 10.5220/0006261003080320
In *Proceedings of the 12th International Joint Conference on Computer Vision, Imaging and Computer Graphics Theory and Applications (VISIGRAPP 2017)*, pages 308-320
ISBN: 978-989-758-227-1

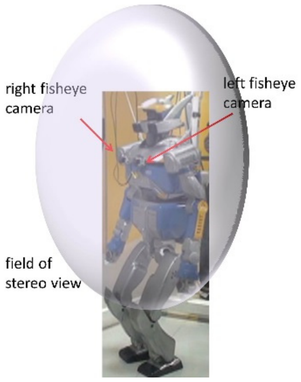

Figure 1: Humanoid robot with fisheye stereo.

Some fisheye lenses have wide fields of view (larger than 180°). Mounting two cameras equipped with such fisheye lenses in parallel on the chest of a humanoid robot yields a stereo field of view greater than 180° with an optical axis that is in the forward direction, as shown in Figure 1. For stereo measurements, stereo correspondence is crucial. However, the distance from the stereo cameras to the target space is short compared with the baseline length of the stereo system; this causes differences in the apparent shapes of the targets in the left and right images. Furthermore, some targets have no clear visual features, which makes stereo correspondence difficult. In this paper, we propose a novel method that rectifies stereo images so that the targets have the same apparent shapes in the left and right images when the targets reside close to a reference plane.

In Section 2 of this paper, we introduce related stereo vision studies and background information related to the proposed method is presented. In Section 3, the proposed rectification method, which is based on a reference plane, is explained. In Section 4, we present the rectification of actual fisheye stereo image pairs using the proposed method by changing the pose of the reference plane while three dimensional measurements are performed using a simple region-based matching method. The experimental results show that using the proposed rectification method yields better results than using other rectification methods when the reference plane is close to the actual target. Finally, in Section 5 we summarize our work and discuss potential future research ideas.

2 RELATED WORKS

In the above section, the necessary measurements to sufficiently evaluate the environment in the immediate vicinity of a robot were detailed. Based on those, there are some conditions that make it difficult to conduct stereo measurements.

D1. The targets are too close (i.e., the distance from the robot is between one to several times that of the stereo baseline length).

D2. The texture of targets is sometimes poor.

D3. The target may lie on an extension of the stereo baseline.

When the target is close to the stereo cameras, its appearance differs greatly between the left and the right image. Similar problems occur even for wide baseline stereo systems, and many methods have been proposed to tackle these problems (Schmid, 1997), (Baumberg, 2000), (Matas, 2004), (Bay, 2005). Most such methods first detect salient features and then derive descriptions that are invariant of the viewing direction. Then the correspondences are taken based on the measure of similarity of the descriptions. The existing methods are not suitable for a target that has no clear visual features.

For a poorly textured target, most methods derive a local description from the intensity changes in the local region and then take correspondences based on the similarity measure of those descriptions (Scharstein, 2002). Several important approaches have been proposed for such region-based methods.

- Epipolar constraint
- Rectification
- Cost function

If the stereo parameters are known, the search region can be constrained on an epipolar line to reduce the risk of mismatching (Hartley, 2003). Further, the left and right images are often transformed so that the epipolar lines coincide with the image rows via rectification (Ayache, 1988), (Courtney, 1992), (Loop, 1999), (Hartley, 1999). Various cost functions have been developed to determine a measure of similarity for local regions (Hirschmuller, 2009). The simplest ones directly utilize the local regions' intensities, e.g., the sum of squared difference (SSD) and normalized SSD (NSSD) functions. Some functions compare descriptors that are derived from the images filtered using Sobel operator, Gauss operator, or other operators (Zabih, 1994), (Geiger, 2010). Complicated functions have primarily been developed to cope with differences in the brightness between the left and right images (Hirschmuller, 2008). Few methods have been developed to handle differences in the apparent shape of objects between the left and right images (Devernay, 1994), (Tola, 2010).

One stereo vision method measures the ragged shape of a ground surface using a fisheye stereo system (Kita, 2011). First a rectification method is used that transforms only the ground portion of the images so that the disparity becomes zero on the expected ground plane. Because the differences in the apparent shapes in the left and right images become small around the ground plane, correspondences can be obtained using simple cost functions even when the texture is poor. This method seems to solve the difficulties D1 and D2. But unfortunately, the rectification method used in that method does not work when the measurement target lies on an extension of the stereo baseline.

Pollefeys used a polar coordinate system to rectify two images that were obtained before and after the camera was moved forward to include two epipoles (Pollefeys, 1999). Abraham also used a polar coordinate system to rectify stereo images that were obtained by two parallel cameras mounted with fisheye lenses (Abraham, 2005). Difficulty D3 can be overcome by using a polar coordinate system, but both methods mentioned above were not conceived to cope with the differences in apparent shape between the left and right images.

In this paper, we therefore propose a new rectification method that combines the approach of achieving zero disparity on a reference plane and the approach of using a polar coordinate system. The advantages of the proposed method are as follows.

- It enables a reference plane to be set on an extension of the stereo baseline.
- Because the differences of the apparent shapes on the left and right images become small for a target that is close to the reference plane, correspondences can be obtained using simple cost functions, even when the texture is poor.

3 REFERENCE PLANE BASED RECTIFICATION METHOD

The proposed method rectifies only a portion of the fisheye images so that the disparity becomes zero on a reference plane. Because something on the reference plane shows the same apparent shape in the left and right rectified images, the correspondence can be detected using a simple region-based matching method with high reliability. Though the reference plane was set manually in the experiments presented in Section 4, in practice it would be set by the humanoid robot at an area that a part of its upper body, e.g., hand, may come in contact with to help it maintain its balance. In the latter part of this section, some coordinate frames are first defined, the method for deciding which part of the fisheye images should be rectified is explained, and finally the method to transform the fisheye images to rectified images is introduced.

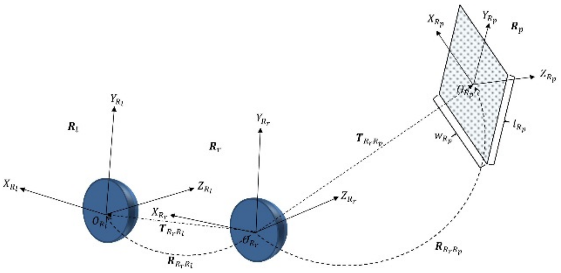

Figure 2: Coordinate frames.

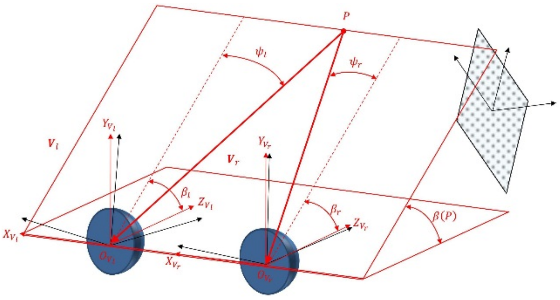

Figure 3: Virtual camera coordinate frames.

3.1 Coordinate Frames

Figure 2 shows left and right fisheye camera coordinates, $\boldsymbol{R}_l$ and $\boldsymbol{R}_r$. Here, for simplicity, $\boldsymbol{R}_r$ is a base frame instead of the world frame. The origins are the optical centers, the *Z* axes are the optical axes, and the *Y* axes are the upper directions of the images (for simplicity, we assume that the image plane is perpendicular to the optical axis). The pose of $\boldsymbol{R}_l$ is represented by the translation $\boldsymbol{T}_{R_rR_l}$ and the rotation $\boldsymbol{R}_{R_rR_l}$, which are assumed to be calibrated in advance. Figure 2 depicts the reference plane. It is a rectangle of size $l_{R_p} \times w_{R_p}$. A coordinate frame $\boldsymbol{R}_p$ is defined as shown in Figure 2. The origin is the center of the rectangle, the *Y* axis is the length direction, the *X* axis is the width direction, and the *Z* axis is the normal direction of the backside of the reference plane. The pose of the reference plane is set by the translation $\boldsymbol{T}_{R_rR_p}$ and the rotation $\boldsymbol{R}_{R_rR_p}$.

Because the cameras must be aligned in parallel to generate the rectified images (Figure 3), the virtual camera coordinate frames, $\boldsymbol{V}_l$ and $\boldsymbol{V}_r$, are defined as follows (Figure 3).

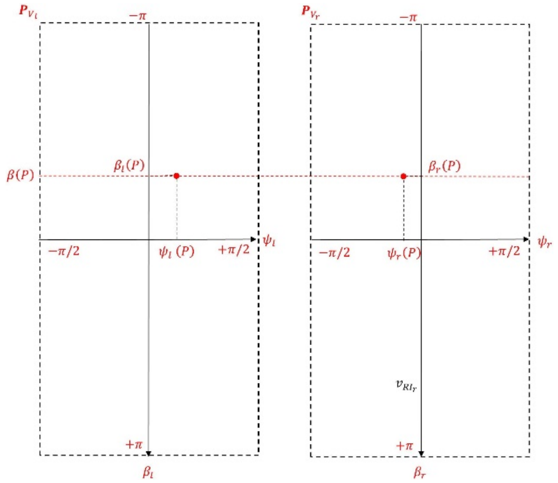

Figure 4: Projection planes.

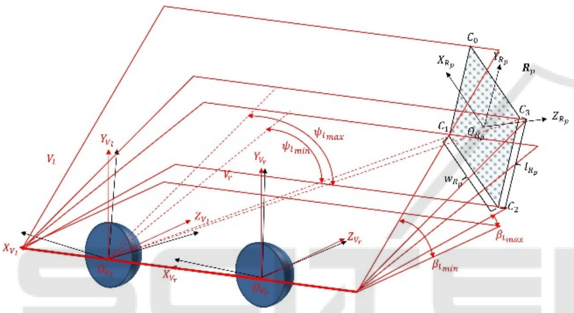

Figure 5: Tilt and yaw angles including a reference plane.

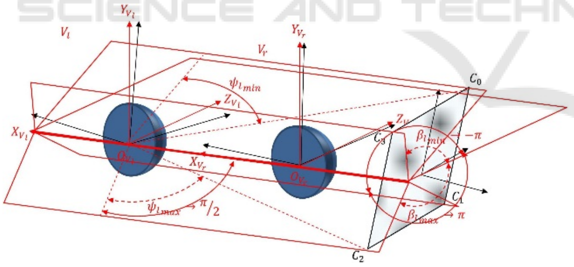

Figure 6: Tilt and yaw angles including a reference plane which crosses an extension of the stereo baseline.

- O_{V_r}coincides with O_{R_r}
- X_{V_r} is the same direction as O_{R_r} to O_{R_l}.
- Y_{V_r} is the direction of the cross product of $Z_{R_r}$and X_{V_r}.
- Z_{V_r} is the direction of the cross product of Y_{V_r} and X_{V_r}.
- $\boldsymbol{V}_l$ is obtained by translating $\boldsymbol{V}_r$ to O_{R_l}.

Let us consider the light rays from a 3D point P to the origins of the left and right virtual cameras, O_{V_l} and O_{V_r}. Their tilt angles $\beta_l(P)$ and $\beta_r(P)$, which are the angles of rotation around the X axes, are equal. This is true for any 3D point. Then, any 3D point is projected at the same vertical position on the left and right projection planes, $\boldsymbol{P}_{V_l}$ and $\boldsymbol{P}_{V_r}$, by relating the vertical positions to the tilt angles. The horizontal positions on the projection planes are related to the yaw angles, $\psi_l(P)$ and $\psi_r(P)$. Here yaw angles are the angles of rotation around the tilted Y axes. For convenience, the tilt angle is defined in the counter clockwise direction from the direction of the Z axes, while the yaw angle is defined in the clockwise direction from the tilted Z direction. The whole 3D space is projected into the area for which the tilt angle ranges from +π to − π and the yaw angle ranges from $-\pi/2$ to $+\pi/2$, as shown in Figure 4.

3.2 Deciding the Rectifying Region

Only the rectangle-shaped portion of the projection plane that contains a projection of the reference plane is rectified rather than the whole projection plane. The rectangle portion that has a tilt angle is from β_{min} to β_{max} and a yaw angle is from ψ_{min} to ψ_{max} is decided in the left projection plane. C_i, for $i = 0,1,2,3$, indicate the four corners of the reference plane, as shown in Figure 5. Their coordinates in the $\boldsymbol{R}_p$ frame are as follows.

$$\begin{aligned} C_{0R_p} &= \left(w_{R_p}/2, l_{R_p}/2, 0\right) \\ C_{1R_p} &= \left(w_{R_p}/2, -l_{R_p}/2, 0\right) \\ C_{2R_p} &= \left(-w_{R_p}/2, -l_{R_p}/2, 0\right) \\ C_{3R_p} &= \left(-w_{R_p}/2, l_{R_p}/2, 0\right) \end{aligned} \tag{1}$$

The C_{iR_p} are converted to the $\boldsymbol{V}_l$ frame through the $\boldsymbol{R}_r$ frame to yield C_{iV_l}. The tilt and yaw angles in the $\boldsymbol{V}_l$ frame can be calculated as follows:

$$\begin{aligned} \beta_{l_i} &= -\tan^{-1}\left(y\left(C_{iV_l}\right)/z\left(C_{iV_l}\right)\right) \\ \psi_{l_i} &= -\sin^{-1}\left(x\left(C_{iV_l}\right)\right) \end{aligned} \tag{2}$$

where $x\left(C_{iV_l}\right)$ represents a X coordinate of C_{iV_l}. Finally, we find that

$$\begin{aligned} \beta_{l_{min}} &= \min_i\{\beta_{l_i} \mid i = 0,1,2,3\} \\ \beta_{l_{max}} &= \max_i\{\beta_{l_i} \mid i = 0,1,2,3\} \\ \psi_{l_{min}} &= \min_i\{\psi_{l_i} \mid i = 0,1,2,3\} \\ \psi_{l_{max}} &= \max_i\{\psi_{l_i} \mid i = 0,1,2,3\} \end{aligned} \tag{3}$$

However, these values are updated when a reference plane crosses an extension of the stereo baseline as follows:

$$\beta_{l_{min}} = -\pi \ \& \ \beta_{l_{max}} = \pi \tag{4}$$

Further, if the X coordinate of the cross point in the frame $\boldsymbol{V}_l$ is positive then $\psi_{l_{min}} = -\pi/2$; otherwise, $\psi_{l_{min}} = \pi/2$, as shown in Figure 6.

3.3 Deciding Pixel Coordinate Frame of Rectified Images

The pixel coordinate frame of the left rectified image, $\boldsymbol{RI}_l$, is defined by equally quantizing the tilt and yaw angles in the left projection plane. The following two issues must be considered to choose the quantizing resolution q_l.

I1. q_l affects the resolution of the 3D depth measurement.

I2. q_l affects p_s, which is the Euclidean distance on a reference plane corresponding to one pixel of the rectified images.

Figure 7 shows how to choose q_l based on the desired depth resolution, h_r. A 3D point Q is set on the light ray from O_{R_p} to O_{V_r} so that the Euclidean distance between Q and the reference plane becomes h_r. The yaw angle of the light ray from Q to O_{V_l} is $\psi_l(Q)$, and one of the light rays from O_{R_p} to O_{V_l} is $\psi_l\left(O_{R_p}\right)$. Then q_l is chosen according to:

$$q_l = \left|\psi_l(Q) - \psi_l\left(O_{R_p}\right)\right| \tag{5}$$

The depth for one pixel disparity becomes about h_r around the center of the reference plane. For issue I2, p_s is calculated as the distance between O_{R_p} and S, which is the intersection between the light ray from Q to O_{V_l} and the reference plane. A larger p_s means a small rectified image. If the calculated p_s is larger than the threshold p_{th}, then point S is moved toward O_{R_p} on the reference plane so that the distance to O_{R_p} becomes p_{th}. q_l is recalculated by using S after it has been moved.

By using the chosen value of q_l, the rectangle region from $\beta_{l_{min}}$n to $\beta_{l_{max}}$ and from $\psi_{l_{min}}$ to $\psi_{l_{max}}$ on the left projection plane is quantized, as shown in Figure 8. The rectangle region on the right projection plane is also quantized vertically using q_l. The rectified image coordinates of a 3D point P, $\left(u_{RI_l},\ v_{RI_l}\right)$ and $\left(u_{RI_r},\ v_{RI_r}\right)$, are obtained from the following equations:

$$\begin{aligned} u_{RI_l}(P) &= (floor)\left(\left(\psi_l(P) - \psi_{l_{min}}\right)/q_l\right) \\ v_{RI_l}(P) &= (floor)\left(\left(\beta_l(P) - \beta_{l_{min}}\right)/q_l\right) \\ v_{RI_r}(P) &= (floor)\left(\left(\beta_r(P) - \beta_{r_{min}}\right)/q_r\right) \end{aligned} \tag{6}$$

Because $\beta_l(P) = \beta_r(P)$, $\beta_{l_{min}} = \beta_{r_{min}}$ and $q_l = q_r$, $v_{RI_l}(P) = v_{RI_r}(P)$ is true for any 3D point P on the rectified image.

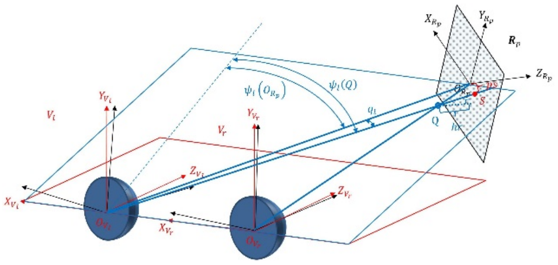

Figure 7: Decision of q_l.

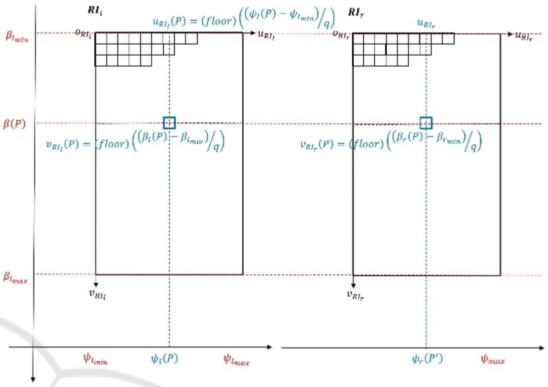
RI_l
$u_{RI_l}(P) = (floor)\left(\left(\psi_l(P) - \psi_{l_{min}}\right)/q\right)$
RI_r
u_{RI_r}
$\beta_{l_{min}}$
O_{RI_l}
u_{RI_l}
O_{RI_r}
u_{RI_r}
$\beta(P)$
$v_{RI_l}(P) = (floor)\left(\left(\beta_l(P) - \beta_{l_{min}}\right)/q\right)$
$v_{RI_r}(P) = (floor)\left(\left(\beta_r(P) - \beta_{r_{min}}\right)/q\right)$
$\beta_{l_{max}}$
v_{RI_l}
v_{RI_r}
$\psi_{l_{min}}$
$\psi_l(P)$
$\psi_{l_{max}}$
$\psi_r(P')$
ψ_{max}

Figure 8: Pixel coordinate frames of rectified images.

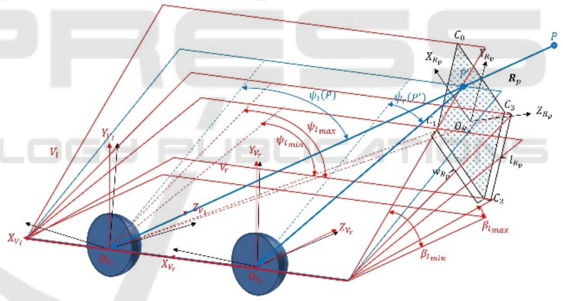

Figure 9: Decision of a yaw angle for the pixel with the coordinates $\left(u_{RI_r}, v_{RI_r}\right)$.

The horizontal quantization of the right projection plane remains to be decided. It is quantized non-linearly so that the disparity becomes zero on the reference plane. The yaw angle in the frame $\boldsymbol{V}_r$ for the pixel with the coordinates $\left(u_{RI_r},\right.$ $\left.v_{RI_r}\right)$ is chosen as follows. First the tilt and yaw angles of the light ray corresponding to the left pixel $\left(u_{RI_l},\ v_{RI_l}\right)$, where $u_{RI_l} = u_{RI_r}$ and $v_{RI_l} = v_{RI_r}$, are obtained via the following equations:

$$\begin{aligned} \beta_l\left(v_{RI_l}\right) &= \left(v_{RI_l} + 0.5\right)\times q_l + \beta_{l_{min}} \\ \psi_l\left(u_{RI_l}\right) &= \left(u_{RI_l} + 0.5\right)\times q_l + \psi_{l_{min}} \end{aligned} \tag{7}$$

Next, the point where the light ray and the reference plane intersect, P’, is obtained as shown in Figure 9.

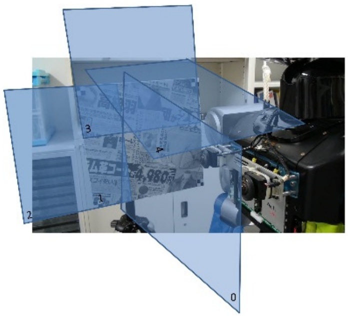

Figure 10: Five poses of target planes.

Finally, the yaw angle in the frame $\boldsymbol{V}_r$ for the pixel with the coordinates (u_{RI_r}, v_{RI_r}) is selected to be $\psi_r(P')$. Using this approach, any 3D point on the reference plane has the same coordinates in the left and right rectified images. This results in the targets having the same apparent shapes in the left and right images when the targets are close to the reference plane.

3.4 Conversion from Fisheye to Rectified Image

For each pixel in the left rectified image, the intensity is obtained as follows. The tilt and yaw angle of the light ray corresponding to the pixel, β_l and ψ_l, are derived using Equation set 7. The unit direction vector for the light ray, L_{V_l}, is obtained according to:

$$L_{V_l} = (\sin(-\psi_l), \cos(-\psi_l)\sin(-\beta_l), \\ , \cos(-\psi_l)\cos(-\beta_l)) \tag{8}$$

L_{R_l} is then obtained by converting L_{V_l} to the $\boldsymbol{R}_l$ frame. The image coordinates in the left fisheye image corresponding to the light ray are calculated as real coordinates using the projection function $Proj_l(L_{R_l})$. Here, all intrinsic parameters of the left fisheye camera were calibrated in advance. From the intensities of the four neighboring pixels in the left fisheye image, the intensity value of the pixel in the left rectified image was calculated via linear interpolation.

For each pixel in the right rectified image, the intensity was obtained in the almost same way as for one in the left rectified image. First, the L_{V_l} for the same coordinate in the left rectified image was obtained. Then, L_{V_l} was converted to L_{R_r} and R_{R_r} was obtained as a light ray from the intersection between L_{R_r} and the reference plane toward O_{R_r}. The image coordinates in the right fisheye image corresponding to the light ray are calculated by the function $Proj_r(R_{R_r})$. From the intensities of the four neighboring pixels in the right fisheye image, the intensity value of the pixel in the right rectified image was calculated via linear interpolation.

4 EXPERIMENTS

The motivation for proposing a new rectification method is to enable 3D distance measurements for targets in close proximity at wide angles, so as to include the line extended from the stereo baseline. Additionally, it should be possible to measure the distances using a simple matching method even when the texture of the targets is poor. Actual fisheye stereo image pairs were rectified using the proposed method, and 3D distance measurements were performed using simple region-based matching on the rectified images. For the comparison, another rectification method was used on the same images and the 3D distances were measured from the rectified images using the same matching method.

4.1 Experimental Setup

The fisheye stereo that was used for the experiments was mounted on the chest of a humanoid robot; the baseline length was about 150 mm and the directions of optical axes were set to point forward, as shown in Figure 1. The field of view of the fisheye lenses were each 214° with an almost spherical projection. The cameras captured the whole viewing field with 1536 × 1536 pixel images.

The targets were two kinds of flat veneer surfaces that were 300 mm × 300 mm in size. One surface was given a rich texture by placing a section of newspaper on it, while the other was left blank and was thus poorly textured. The targets were fixed at five poses as shown in Figure 10. The poses were chosen such that they were in poses that the humanoid robot would be able to touch with its right hand to stabilize itself. The positions and orientations of the five poses were as follows.

Pose 0. (75, 0, 200), (0, 0, 0),
Pose 1. (−200, 0, 100), (0, −90, 0),
Pose 2. (−200, 0, 300), (0, −90, 0),
Pose 3. (−200, 200, 100), (0, −90, 0),
Pose 4. (75, 250, 100), (−90, 0, 0).

The positions and orientations were based on the frame $\boldsymbol{R}_r$, which is the same as for the reference plane. The position coordinates are given in millimeters, while the orientations are given in degrees. The orientation is represented by YXZ

Euler angles. Because it was difficult to fix the targets at the intended poses, the actual poses were slightly different and the actual poses that were measured using the method described in Section 4.4 are shown in Table 1. For convenience, a name is given to each pair of stereo images, e.g., 0-rich-0, where the first number represents a pose between 0 and 4, the second indicates the surface type (rich or poor, i.e., richly or poorly textured), and the third number represents the orientation (0–4). The orientation numbers have the following significance:

0: base orientation
1: rotate 0 about 10° around Y axis
2: rotate 0 about −10° around Y axis
3: rotate 0 about 10° around X axis
4: rotate 0 about −10° around X axis

The rich and poor input image pairs at the five poses with the base orientations are shown in Figure 11. The images were captured for orientation 0 for every position. Only for positons 0 and 1 were the images captured for orientations 1 to 4.

4.2 Rectification of Fisheye Images

In the proposed rectification method a reference plane is set to decide which portion of the fisheye images should be rectified. The size of rectified images is determined by setting a desired depth resolution, h_r, and a threshold for p_s, p_{th}. The process introduced in Section 3.4 generates rectified images based on the reference plane. Here three typical examples are presented.

Example 1. Dimensions of a reference plane: $l_{R_p} = 250$, $w_{R_p} = 250$. Pose: $\boldsymbol{T}_{R_rR_p} = (75, 0, 200)$, $\boldsymbol{R}_{R_rR_p} = (0, 0, 0)$. Further, $\beta_{l_{min}}$ is -51.2, $\beta_{l_{max}} = 49.6$, $\psi_{l_{min}} = -17.6$, and $\psi_{l_{max}} = 52.3$. h_r and p_{th} are set to 10 and 2, respectively. Now p_s is 2.11. Because this is larger than p_{th}, h_r is updated to 1.3 so that p_s is equal to p_{th}. Then, q_l is 0.684 and the size of the rectified images is 124 × 172. Generated rectified images from 0-rich-0 are shown in Figure 12(a).

Example 2. Dimensions of a reference plane: $l_{R_p} = 250$, $w_{R_p} = 250$. Pose: $\boldsymbol{T}_{R_rR_p} = (-200, 0, 100)$, $\boldsymbol{R}_{R_rR_p} = (0, -90, 0)$. Further, $\beta_{l_{min}}$ is $-\pi$, $\beta_{l_{max}} = \pi$, $\psi_{l_{min}} = 50.9$, and $\psi_{l_{max}} = 73.1$. h_r and p_{th} are set to 10 and 2, respectively. Now p_s is 2.11. Because this is larger than p_{th}, h_r is updated to 9.49 so that p_s is equal to p_{th}. Then, q_l is 0.297 and the size of the rectified images is 152 × 1232. Generated rectified images from 1-rich-0 are shown in Figure 12(b).

Table 1: Target poses and reference plane poses.

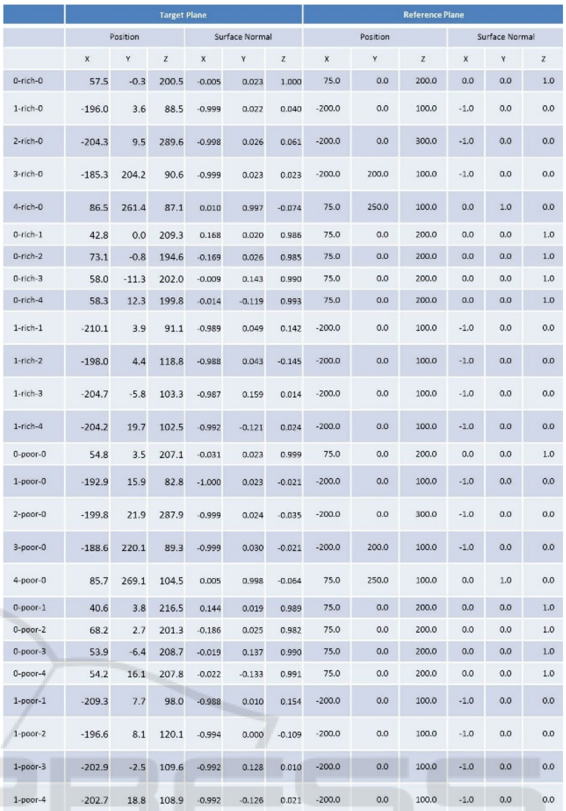

	Target Plane						Reference Plane					
	Position			Surface Normal			Position			Surface Normal		
	X	Y	Z	X	Y	Z	X	Y	Z	X	Y	Z
0-rich-0	57.5	-0.3	200.5	-0.005	0.023	1.000	75.0	0.0	200.0	0.0	0.0	1.0
1-rich-0	-196.0	3.6	88.5	-0.999	0.022	0.040	-200.0	0.0	100.0	-1.0	0.0	0.0
2-rich-0	-204.3	9.5	289.6	-0.998	0.026	0.061	-200.0	0.0	300.0	-1.0	0.0	0.0
3-rich-0	-185.3	204.2	90.6	-0.999	0.023	0.023	-200.0	200.0	100.0	-1.0	0.0	0.0
4-rich-0	86.5	261.4	87.1	0.010	0.997	-0.074	75.0	250.0	100.0	0.0	1.0	0.0
0-rich-1	42.8	0.0	209.3	0.168	0.020	0.986	75.0	0.0	200.0	0.0	0.0	1.0
0-rich-2	73.1	-0.8	194.6	-0.169	0.026	0.985	75.0	0.0	200.0	0.0	0.0	1.0
0-rich-3	58.0	-11.3	202.0	-0.009	0.143	0.990	75.0	0.0	200.0	0.0	0.0	1.0
0-rich-4	58.3	12.3	199.8	-0.014	-0.119	0.993	75.0	0.0	200.0	0.0	0.0	1.0
1-rich-1	-210.1	3.9	91.1	-0.989	0.049	0.142	-200.0	0.0	100.0	-1.0	0.0	0.0
1-rich-2	-198.0	4.4	118.8	-0.988	0.043	-0.145	-200.0	0.0	100.0	-1.0	0.0	0.0
1-rich-3	-204.7	-5.8	103.3	-0.987	0.159	0.014	-200.0	0.0	100.0	-1.0	0.0	0.0
1-rich-4	-204.2	19.7	102.5	-0.992	-0.121	0.024	-200.0	0.0	100.0	-1.0	0.0	0.0
0-poor-0	54.8	3.5	207.1	-0.031	0.023	0.999	75.0	0.0	200.0	0.0	0.0	1.0
1-poor-0	-192.9	15.9	82.8	-1.000	0.023	-0.021	-200.0	0.0	100.0	-1.0	0.0	0.0
2-poor-0	-199.8	21.9	287.9	-0.999	0.024	-0.035	-200.0	0.0	300.0	-1.0	0.0	0.0
3-poor-0	-188.6	220.1	89.3	-0.999	0.030	-0.021	-200.0	200.0	100.0	-1.0	0.0	0.0
4-poor-0	85.7	269.1	104.5	0.005	0.998	-0.064	75.0	250.0	100.0	0.0	1.0	0.0
0-poor-1	40.6	3.8	216.5	0.144	0.019	0.989	75.0	0.0	200.0	0.0	0.0	1.0
0-poor-2	68.2	2.7	201.3	-0.186	0.025	0.982	75.0	0.0	200.0	0.0	0.0	1.0
0-poor-3	53.9	-6.4	208.7	-0.019	0.137	0.990	75.0	0.0	200.0	0.0	0.0	1.0
0-poor-4	54.2	16.1	207.8	-0.022	-0.133	0.991	75.0	0.0	200.0	0.0	0.0	1.0
1-poor-1	-209.3	7.7	98.0	-0.988	0.010	0.154	-200.0	0.0	100.0	-1.0	0.0	0.0
1-poor-2	-196.6	8.1	120.1	-0.994	0.000	-0.109	-200.0	0.0	100.0	-1.0	0.0	0.0
1-poor-3	-202.9	-2.5	109.6	-0.992	0.128	0.010	-200.0	0.0	100.0	-1.0	0.0	0.0
1-poor-4	-202.7	18.8	108.9	-0.992	-0.126	0.021	-200.0	0.0	100.0	-1.0	0.0	0.0

Example 3. Dimensions of a reference plane: $l_{R_p} = 250$, $w_{R_p} = 250$. Pose: $\boldsymbol{T}_{R_rR_p} = (-200, 300, 100)$, $\boldsymbol{R}_{R_rR_p} = (0, -90, 0)$. Further, $\beta_{l_{min}}$ is -95.7, $\beta_{l_{max}}$ = -20.7, $\psi_{l_{min}}$ = 38.9, and $\psi_{l_{max}}$ = 75.4. h_r and p_{th} are set to 10 and 2, respectively. Now p_s is 4.83. Because this is larger than p_{th}, h_r is updated to 4.21 so that p_s is equal to p_{th}. Then, q_l is 0.228 and the size of the rectified images is 184 × 352. Generated rectified images from 3-rich-0 are shown in Figure 12(c).

Because the reference planes are set close to the actual targets in all three examples, the apparent shape of the targets on the rectified images are quite similar.

For comparison, another rectification method was implemented by referring to Abraham. This method rectifies fisheye images of the whole projection plane with equal quantization amounts q_l for both the vertical and horizontal directions. Thus, the typical difference in the implementation of this method and the proposed method is the relation between the yaw angles and the horizontal pixel coordinates on the right rectified image according to

$$u_{RI_r}(P) = (floor)\left(\left(\psi_r(P) - \psi_{r_{min}}\right)/q_l\right) \tag{9}$$

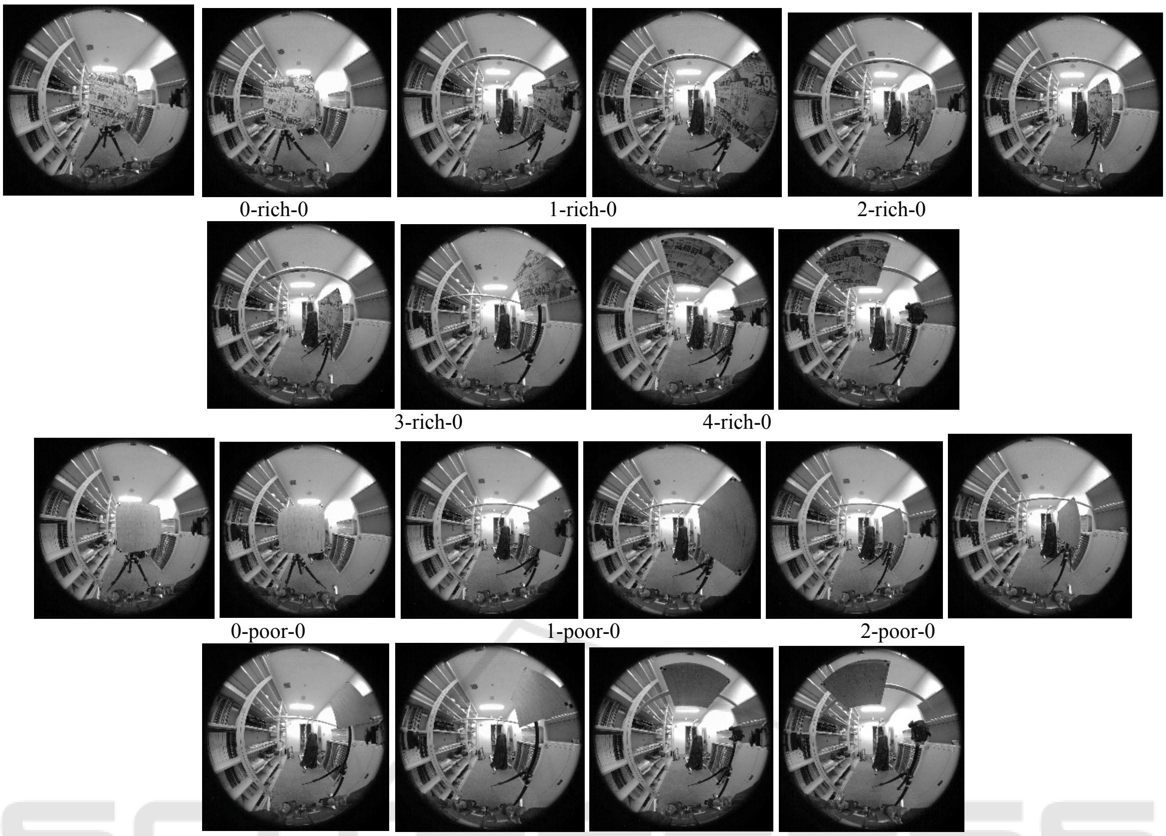

0-rich-0 1-rich-0 2-rich-0

3-rich-0 4-rich-0

0-poor-0 1-poor-0 2-poor-0

3-poor-0 4-poor-0

Figure 11: Input fisheye images.

For the remainder of this paper, this rectification is referred to as the Abraham method. As for the above Examples 1, 2, and 3, the Abraham method was applied to 0-rich-0, 1-rich-0, and 3-rich-0 and the generated rectified images are shown in Figure 13. The obtained quantization amount q_l was the same as with the proposed method with a reference plane and the two parameters h_r and p_{th}. The sizes of the rectified images are 396 × 768, 628 × 1232, and 812 × 1604.

4.3 3D Distance Measurements

In the rectified images, corresponding pairs were identified with a region-based method using NSSD (Davison, 1998) as the measure of dissimilarity. The necessary parameters are listed here.

patch_size: the size of the local region where the NSSD is calculated. Here it was 21 pixel.

corr_th: threshold of the dissimilarity for acceptance as a matching pair. Here it was 1.5.

corr_diff_th: threshold of the saliency for acceptance as a matching pair. Here it was 0.5.

max_d: search was performed within this distance from the reference plane. Here it was 200 mm.

For each pixel in the left rectified image, stereo matching is carried out as follows if the corresponding light ray crosses with the reference plane. Between pixel (u, v) in the left rectified image and the pixels in the right rectified images that have the same v and lie between $\left(u - (max\_d/h_r)\right)$ and $\left(u + (max\_d/h_r)\right)$, the NSSD was calculated for the local region with a size: *patch_size* × *patch_size*. If the minimum value of the NSSDs is lower than *corr_th* and the differences between the NSSDs of the horizontal neighbors are larger than *corr_diff_th*, the pixel is a matching candidate. Using the same process, the matching candidate in the left rectified image is determined via a reverse searched from the matching candidates in the right rectified image. If the found pixel is (u, v), the pair is as a matching pair.

For the images rectified by the Abraham method, the same procedure with the same parameters was applied with only one exception: the search area was defined as lying between $\left(u + d - (max\_d/h_r)\right)$

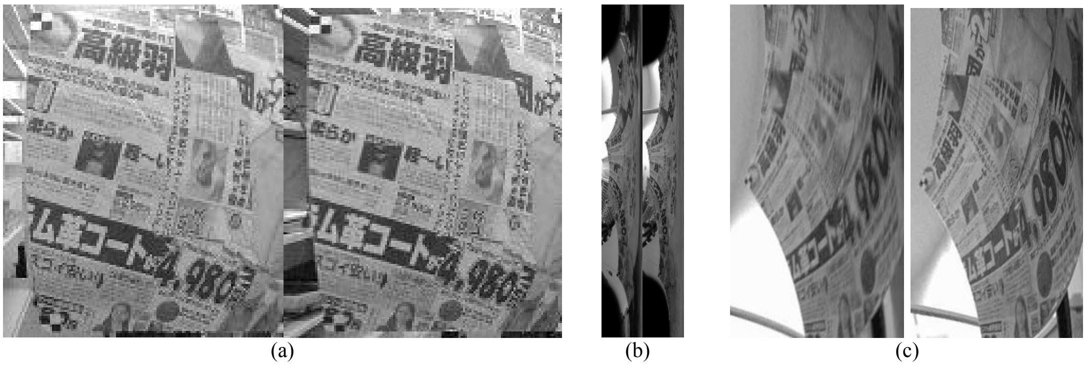

Figure 12: Rectified images by the proposed method.

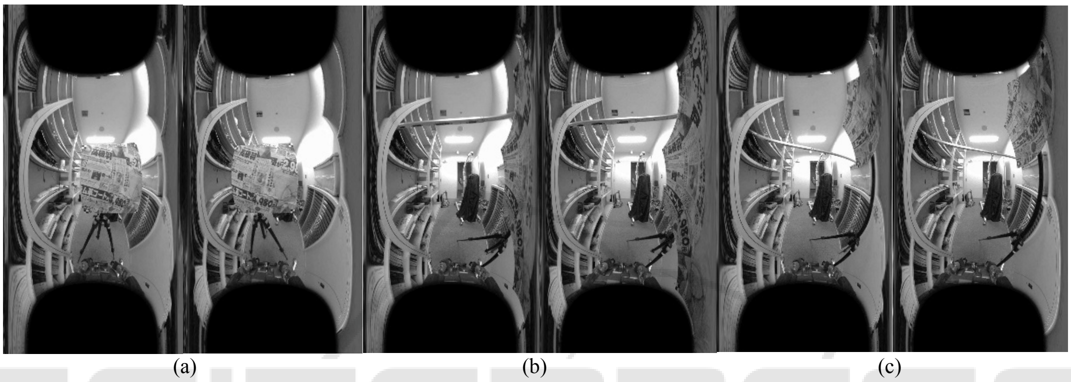

Figure 13: Rectified images by Abraham method.

and $(u + d + (max\_d/h_r))$ by using d, which is the disparity on the reference plane.

For the matching pairs, the 3D location was calculated as the crossing point of the corresponding left and right rays.

4.4 Evaluation Criteria

The total number, *TN*, is defined as the number of the pixels for which the stereo matching was carried out. The matching number, *MN*, is defined as the number of matching pairs. The correct number, *CN*, is defined as the number of matching pairs from which a 3D location is calculated and for which the distance between it and the actual target plane was less than the threshold, d_{th} . The following evaluation criteria were used:

MN/TN,

CN/MN.

The actual pose of the target plane was obtained from the left and right fisheye images by detecting the cross marks, ▚ , that were placed at the four corners of the target. The threshold d_{th} was 10 mm.

4.5 Experimental Results

Figure 14 shows the results obtained from the fisheye image pairs at the five poses with the base orientation. Figure 15 shows the results obtained from the fisheye image pairs at pose 0 with the five orientations. Figure 16 shows the results obtained from the fisheye image pairs at pose 1 with the five orientations. Blue represents the results obtained by using the proposed rectification method and orange represents the results obtained using the Abraham method. The + symbols indicate the values of *MN/TN* × 100, while the ■ symbols represent the values of *CN/MN* × 100. For each input image pair, the 3D distances were measured nine times for various reference plane positions. The numbers from −4 to 4 on the horizontal axis, *k*, correspond to the positions of the reference planes, where 0 is the base position, which is the closest to the actual target plane. –*k* means that the reference plane is moved toward the cameras along the normal direction of the reference plane at (*k* × 25) mm from the base position. +*k* means that the reference plane is moved away from the cameras along the normal direction of the reference plane at (*k* × 25) mm from the base

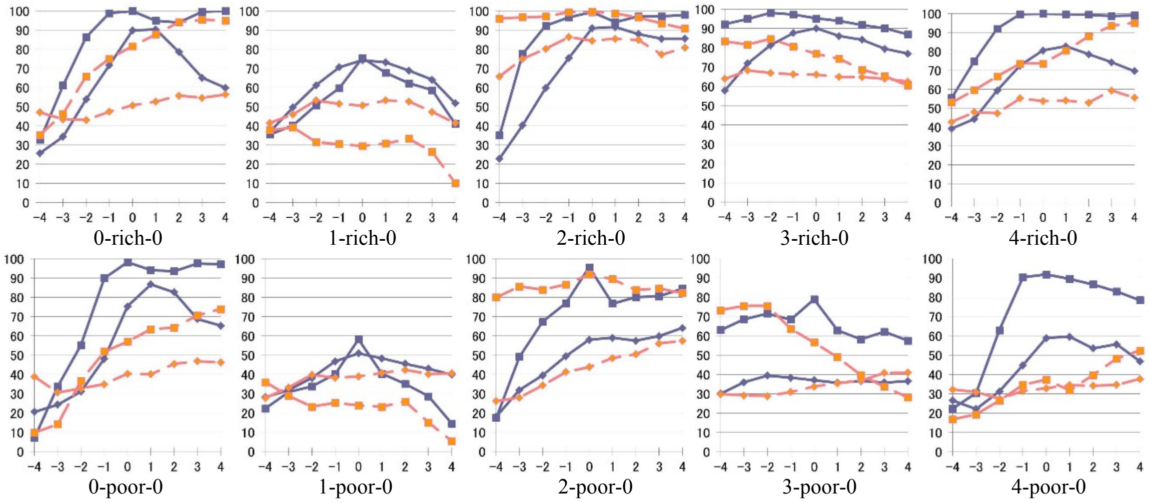

0-rich-0 1-rich-0 2-rich-0 3-rich-0 4-rich-0

0-poor-0 1-poor-0 2-poor-0 3-poor-0 4-poor-0

Figure 14: Results obtained from the fisheye image pairs at the five poses with the base orientation.

position. To obtain the results for Figures 15 and 16, the same reference plane orientation was used independent of the actual orientation of the target. Table 1 shows the actual pose of targets and the pose of reference planes at the base position.

Prior to conducting the experiments, the following five phenomena were predicted to occur.

E1. With the proposed method, the results should worsen as |*k*| increases.

E2. With the Abraham method, the results should be almost constant independent of |*k*|.

E3. The results of the proposed method should be better than ones of the Abraham method when |*k*| is small.

E4. The results for poor textures should be worse than for rich textures; however, for positions at which |*k*| is small, reasonable results should be obtained using the proposed method.

E5. The effect of the orientation difference between the target and reference planes should be much smaller than that caused by the positional difference between the target and reference planes.

Based on the results shown in Figure 14, the expectations E1 to E4 are supported as follows. E1 was true for pose 0. For poses 0, 2, and 4 the results for larger *k* did not worsen and for pose 3 the results did not change significantly regardless of the values of *k*. E2 was not true; the results monotonically increased or decreased along with the positional changes. This seems to be caused by the changes in the amount of quantization. E3 held true except for pose 2. Figure 17 depicts the changes in Euclidean distance on the reference plane corresponding to one pixel when the yaw angles are equally quantized on the left and right rectified images, as in the Abraham method. Figure 17(a) is for pose 0 and (b) for pose 2. As seen in Figure 17(a), the Euclidean distances on the reference plane corresponding to one pixel were quite different between the left and right images; this causes the difference in the apparent shape in the rectified images even when the target resides on the reference plane. Conversely, for pose 2, the Euclidean distances on the reference plane corresponding to one pixel were almost the same between the left and right images, which causes apparent shape in the left and right rectified images to be similar even when the target is not on the reference plane. This causes the results for pose 2 at any position using the Abraham method to be almost the same as those obtained at position 0 using the proposed method. As expected according to E4, the results for the poor texture were worse than those for the rich texture for both the Abraham and the proposed method. For pose 1, which is the most challenging configuration for a stereo measurement, the *CN/MN* was less than 25% for the Abraham method. Conversely, using the proposed method, the *CN/MN* was greater than 40% for |*k*| < 2. Figure 18 shows the results of the 3D distance measurements for pose 1 of poor texture. The upper two rows are for the proposed method and the lower two rows are for the Abraham method. White solid rectangles indicate the cameras. The white solid lines show the viewing directions of the cameras. Further, white dots represent the measured results. Additionally, the red squares show the reference planes. Estimating whether a real plane does or does not exist in the measurement area and estimating the pose of the plane if it does exist appears to be difficult to achieve from the point clouds obtained by the Abraham method. However, from the point

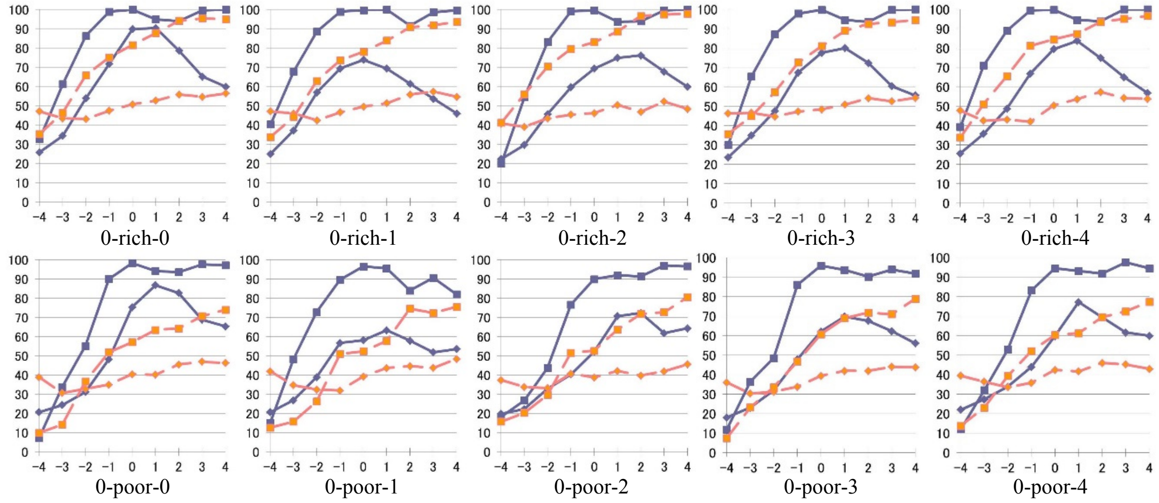

0-rich-0 0-rich-1 0-rich-2 0-rich-3 0-rich-4

0-poor-0 0-poor-1 0-poor-2 0-poor-3 0-poor-4

Figure 15: Results obtained from the fisheye image pairs at pose 0 with the five orientations.

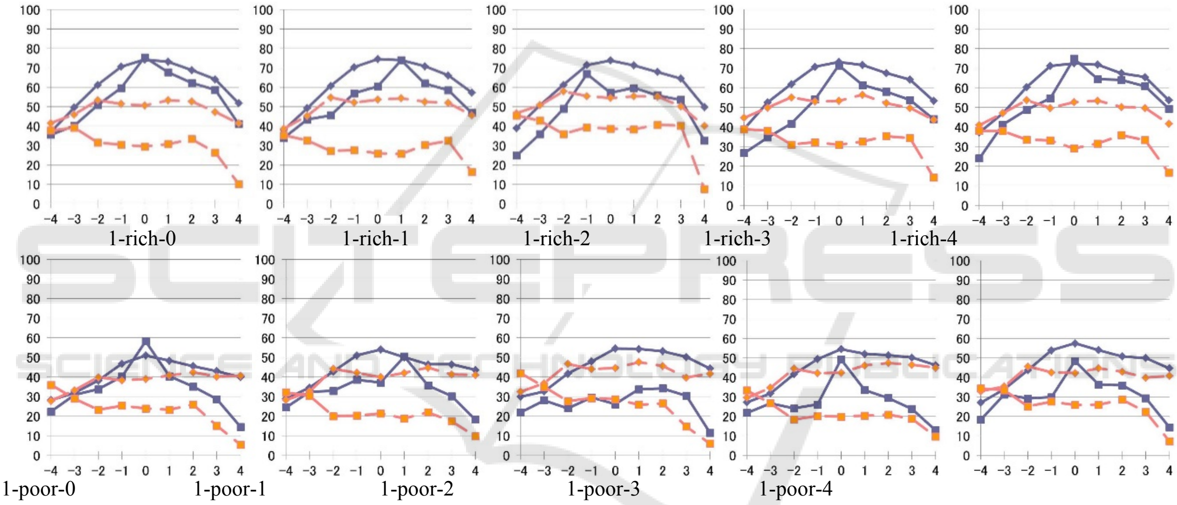

1-rich-0 1-rich-1 1-rich-2 1-rich-3 1-rich-4

1-poor-0 1-poor-1 1-poor-2 1-poor-3 1-poor-4

Figure 16: Results obtained from the fisheye image pairs at pose 1 with the five orientations.

clouds obtained by the proposed method for $|k| < 2$, making such an estimation appears to be possible with only simple post processing.

Based on the results shown in Figures 15 and 16, E5 is true.

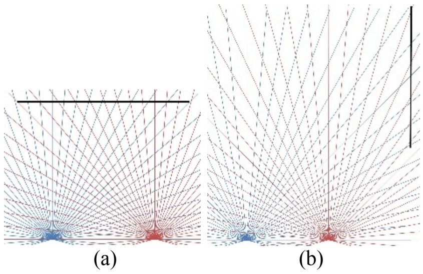

(a) (b)

Figure 17: Changes in Euclidean distance on the reference plane corresponding to one pixel when the yaw angles are equally quantized on the left and right rectified images.

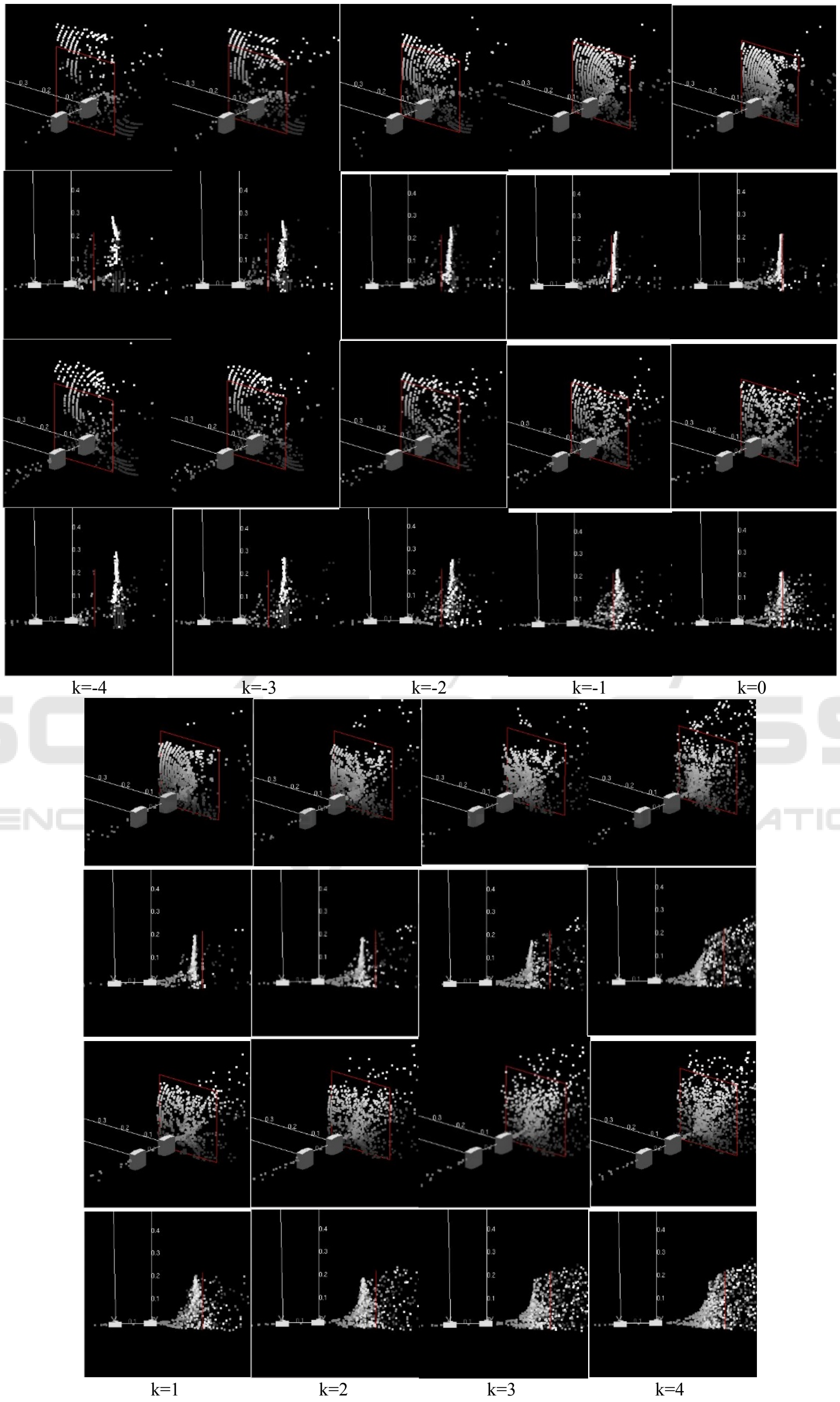

Figure 18: Results of the 3D distance measurements for pose 1 of poor texture.

5 CONCLUSIONS

We proposed a new epipolar rectification method for fisheye images. It rectifies a portion of the fisheye images so that the apparent shape on the left and right rectified images becomes similar if a target is close to a reference plane. By using the proposed method and setting the reference plane appropriately, the 3D distances of a target plane can be measured using a simple region-based matching method, even if the target plane lies within reach of the robot to which the cameras are mounted and even if it lies in the direction of the extension of the stereo baseline. The superiority of the proposed method was experimentally compared with another method to validate it.

We are now developing a method to judge the existence of a plane and estimate the pose of the plane should it exist based on the proposed method; this method will be applied for the motion planning of a humanoid robot when it needs to contact any part of its upper body with the environment to retain its balance.

REFERENCES

Sentis, L., 2010. Compliant control of whole-body multi-contact behaviors in humanoid robots. Motion Planning for Humanoid Robots, Springer: 29-66.

Escande, A., A. Kheddar, et al., 2013. Planning contact points for humanoid robots. Robotics and Autonomous Systems 61(5): 428-442.

Henze, B., M. A. Roa, et al., 2016. Passivity-based whole-body balancing for torque-controlled humanoid robots in multi-contact scenarios. The International Journal of Robotics Research: 0278364916653815.

Brossette, S., J. Vaillant, et al., 2013. Point-cloud multi-contact planning for humanoids: Preliminary results. 6th IEEE Conference on Robotics, Automation and Mechatronics (RAM), IEEE.

Khatib, O. and S.-Y. Chung, 2014. SupraPeds: Humanoid contact-supported locomotion for 3D unstructured environments. IEEE International Conference on Robotics and Automation (ICRA), IEEE.

Schmid, C. and A. Zisserman, 1997. Automatic line matching across views. Computer Vision and Pattern Recognition..

Baumberg, A., 2000. Reliable feature matching across widely separated views. Computer Vision and Pattern Recognition.

Matas, J., O. Chum, et al., 2004. Robust wide-baseline stereo from maximally stable extremal regions. Image and vision computing 22(10): 761-767.

Bay, H., V. Ferrari, et al., 2005. Wide-baseline stereo matching with line segments. Computer Vision and Pattern Recognition.

Scharstein, D. and R. Szeliski, 2002. A taxonomy and evaluation of dense two-frame stereo correspondence algorithms. International Journal of Computer Vision 47(1-3): 7-42.

Hartley, R. and A. Zisserman, 2003. Multiple view geometry in computer vision, Cambridge university press.

Ayache, N. and C. Hansen, 1988. Rectification of images for binocular and trinocular stereovision. 9th International Conference on Pattern Recognition.

Courtney, P., N. A. Thacker, et al., 1992. A Hardware Architecture for Image Rectification and Ground Plane Obstacle Avoidance. Proc. 11th ICPR 1992.

Loop, C. and Z. Zhang, 1999. Computing rectifying homographies for stereo vision. Computer Vision and Pattern Recognition.

Hartley, R. I., 1999. Theory and Practice of Projective Rectification. Int. J. Comput. Vision 35(2): 115-127.

Hirschmuller, H. and D. Scharstein, 2009. Evaluation of stereo matching costs on images with radiometric differences. IEEE Transactions on Pattern Analysis and Machine Intelligence 31(9): 1582-1599.

Zabih, R. and J. Woodfill, 1994. Non-parametric local transforms for computing visual correspondence. European conference on computer vision, Springer.

Geiger, A., M. Roser, et al., 2010. Efficient large-scale stereo matching. Asian conference on computer vision, Springer.

Hirschmuller, H., 2008. Stereo processing by semiglobal matching and mutual information. IEEE Transactions on Pattern Analysis and Machine Intelligence 30(2): 328-341.

Devernay, F. and O. D. Faugeras, 1994. Computing differential properties of 3-D shapes from stereoscopic images without 3-D models. Computer Vision and Pattern Recognition.

Tola, E., V. Lepetit, et al., 2010. Daisy: An efficient dense descriptor applied to wide-baseline stereo. Pattern Analysis and Machine Intelligence, IEEE Transactions on 32(5): 815-830.

Kita, N., 2011. Direct floor height measurement for biped walking robot by fisheye stereo. 11th IEEE-RAS International Conference on Humanoid Robots.

Pollefeys, M., R. Koch, et al., 1999. A simple and efficient rectification method for general motion. The Proceedings of the Seventh IEEE International Conference on Computer Vision.

Abraham, S. and W. Förstner, 2005. Fish-eye-stereo calibration and epipolar rectification. ISPRS Journal of Photogrammetry and Remote Sensing 59(5): 278-288.

Davison, A., 1998. Mobile Robot Navigation Using Active Vision. D. Phil Thesis, University of Oxford.